

Non-radiative complete surface acoustic wave bandgap for finite-depth holey phononic crystal in lithium niobate

Didit Yudistira, Yan Pennec, Bahram Djafari Rouhani, Samuel Dupont, and Vincent Laude

Citation: *Appl. Phys. Lett.* **100**, 061912 (2012); doi: 10.1063/1.3684839

View online: <http://dx.doi.org/10.1063/1.3684839>

View Table of Contents: <http://apl.aip.org/resource/1/APPLAB/v100/i6>

Published by the [American Institute of Physics](http://www.aip.org).

Related Articles

Surface acoustic wave micromotor with arbitrary axis rotational capability

Appl. Phys. Lett. **99**, 214101 (2011)

Guided propagation of surface acoustic waves and piezoelectric field enhancement in ZnO/GaAs systems

J. Appl. Phys. **110**, 103501 (2011)

Cut-off frequencies of Lamb waves in various functionally graded thin films

Appl. Phys. Lett. **99**, 121907 (2011)

Theoretical analysis of ultrahigh electromechanical coupling surface acoustic wave propagation in Pb(In_{1/2}Nb_{1/2})O₃-Pb(Mg_{1/3}Nb_{2/3})O₃-PbTiO₃ crystals

J. Appl. Phys. **109**, 054104 (2011)

Acoustic confinement and waveguiding with a line-defect structure in phononic crystal slabs

J. Appl. Phys. **108**, 084515 (2010)

Additional information on *Appl. Phys. Lett.*

Journal Homepage: <http://apl.aip.org/>

Journal Information: http://apl.aip.org/about/about_the_journal

Top downloads: http://apl.aip.org/features/most_downloaded

Information for Authors: <http://apl.aip.org/authors>

ADVERTISEMENT



LakeShore Model 8404 developed with **TOYO Corporation**
NEW AC/DC Hall Effect System Measure mobilities down to 0.001 cm²/V s

Non-radiative complete surface acoustic wave bandgap for finite-depth holey phononic crystal in lithium niobate

Didit Yulistira,^{1,(a)} Yan Pennec,¹ Bahram Djafari Rouhani,¹ Samuel Dupont,² and Vincent Laude³

¹*Institut d'Electronique, de Microélectronique et de Nanotechnologie (IEMN), UMR CNRS 8520, Université de Lille 1, 59655 Villeneuve d'Ascq Cedex, France*

²*Institut d'Electronique, de Microélectronique et de Nanotechnologie (IEMN), UMR CNRS 8520, UVHC, F-59313 Valenciennes, France*

³*Institut FEMTO-ST, CNRS, ENSMM, UTBM, Université de Franche-Comté, 32 Avenue de l'Observatoire, F-25044 Besançon, France*

(Received 16 December 2011; accepted 24 January 2012; published online 10 February 2012)

We demonstrate the existence of non-radiative complete surface acoustic wave (SAW) bandgaps for two-dimensional piezoelectric phononic crystals of holes. Holes of finite depth in a semi-infinite LiNbO₃ substrate are specifically considered. SAW bandgaps are determined from the band structure calculated with a three-dimensional finite element method taking into account material anisotropy and piezoelectricity. The effect of hole geometry on the bandgaps has been investigated. It is further found that the complete band gap does not close for moderately conical holes. © 2012 American Institute of Physics. [doi:10.1063/1.3684839]

Phononic crystals (PCs) have drawn significant attention since the beginning of the 1990s, as they offer a possibility to control acoustic wave propagation at the wavelength scale, thanks to their ability to exhibit phononic (or acoustic) bandgaps.^{1,2} Bandgaps are the ranges of frequency inside which the propagation of acoustic waves through the PC is forbidden. Such control has made it possible to achieve interesting acoustic structures, such as acoustic waveguides³ or acoustic metamaterials,⁴ among others. PC has led to several interesting applications, such as lab-on-chip for bio-analysis⁵ or phononic crystals when they are combined with photonic crystals.⁶ In some instances, e.g., in the case of acoustic waveguides, the existence of a complete acoustic bandgap extending throughout the first Brillouin zone is of paramount importance. Many PC configurations supporting complete bandgaps have been proposed.^{7,8} Most works, however, have focused mostly on bandgaps for bulk waves, or for Lamb acoustic waves in periodic plates, for instance drilled with holes⁹ or possibly supporting pillars.¹⁰ Non-radiative complete bandgaps for surface acoustic waves (SAWs), in contrast, have attracted less attention, despite widespread use of SAW in the field of wireless telecommunications. Moreover, the ease of exciting SAW with interdigitated transducers (IDTs) or superlattice based transducers¹¹ on a piezoelectric substrate could yield monolithic PC based devices.

The first consideration of SAW on semi-infinite two-dimensional (2D) non-piezoelectric PC with circular inclusions was reported in Ref. 12. Based on a similar configuration, Ref. 13 predicted that a piezoelectric PC with a square lattice of semi-infinite holes on Y-cut LiNbO₃ substrate can exhibit a full SAW bandgap. The experimental demonstration that followed, however, indicated that significant losses could appear for frequencies above the bandgap,¹⁴ an effect that was not predicted by the aforementioned theory.

Such losses were later explained by the finite depth of the holes in the practical PC structure.¹⁵ Radiation losses are indeed expected for frequencies lying inside the sound cone of the LiNbO₃ substrate, as defined by the sound line. The sound line is determined from the dispersion relation of the slowest bulk wave of the substrate. Radiation, thus, results from the coupling of SAW with substrate modes.¹⁵ Although complete SAW bandgaps have been found in the case of pillars on a surface,^{16,17} in which case a complete SAW bandgap can be found for frequencies far below the sound line as a result of the locally resonant mechanism, there has not been any theoretical demonstration of a non-radiative complete SAW bandgap for monolithic piezoelectric PC made of finite depth holes.

In this letter, we report a non-radiative complete SAW band gap exhibited by a 2D piezoelectric PC made of finite depth holes on a semi-infinite LiNbO₃ substrate. The array of holes constituting the PC is arranged according to a honeycomb lattice. We show that, for given geometrical parameters of the holes, the SAW bandgap can be located well under the sound cone of the LiNbO₃ substrate and that a complete bandgap is obtained. We first present SAW band structures calculated by means of a 3D finite element method (FEM). In the numerical simulations, a finite depth is considered for the holes, unlike in previous studies.¹³ The slowness curves for the bulk waves of the LiNbO₃ substrate, taking into account both piezoelectricity and anisotropy, are considered in order to define the relevant irreducible Brillouin zone. Next, we investigate the effect of the geometry of the hole and we evaluate the effect of a conical shape on the behaviour of SAW bandgap.

Figure 1(a) shows a top view of a typical 2D PC structure with honeycomb lattice. The corresponding unit cell is illustrated by Fig. 1(b) in a 3D representation. The unit cell, with lattice constant a , includes two identical holes with diameter d and depth h , embedded in a Y-cut LiNbO₃ crystal substrate. The crystallographic axes of the substrate are such that Y and Z are aligned with the x_3 -axis and the x_2 -axis of

^{a)} Author to whom correspondence should be addressed. Electronic mail: Didit.Yulistira@iemn.univ-lille1.fr.

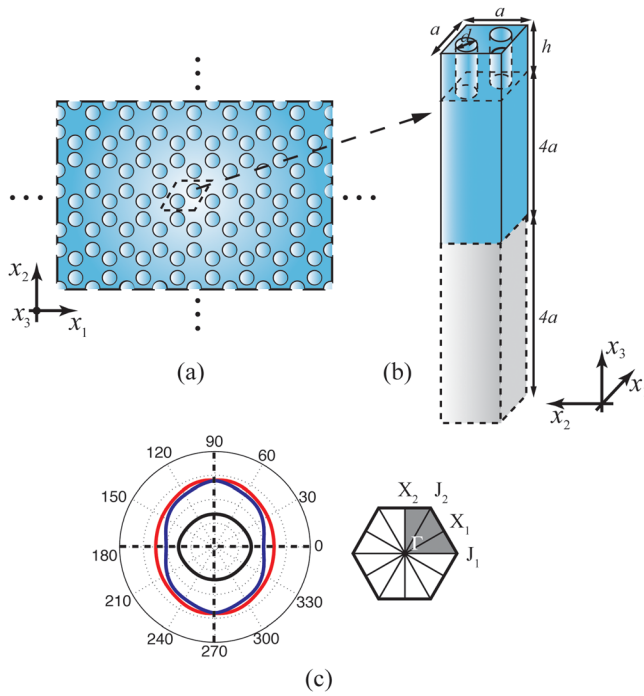


FIG. 1. (Color online) (a) Top view of a 2D piezoelectric PC composed of an air hole array arranged according to a honeycomb lattice. (b) 3D representation of the unit cell where the blue and the grey areas denote the LiNbO₃ layer and the artificial layer, respectively. (c) Slowness curves of Y-cut LiNbO₃ (left) and first Brillouin zone of the honeycomb lattice (right). The black, the dark blue, and the red lines correspond to the different bulk waves in LiNbO₃, while the dashed lines indicate the symmetries of the LiNbO₃ crystal. The dark grey area is the first irreducible Brillouin zone with combined material and lattice symmetries.

the PC, respectively. In the finite element model, taking into account the fact that the penetration depth of SAW is roughly one-wavelength from the surface, the thickness of a layer accounting for the substrate was taken to be four times the lattice constant, or $4a$. Furthermore, to avoid the excitation of spurious modes under the sound cone, particularly, the SAW that may propagate at the free bottom surface of the LiNbO₃ layer, an additional $4a$ -thick artificial layer with high acoustic velocities when compared with those of LiNbO₃ was introduced, as shown in Fig. 1(a). This layer is designed to allow only the excitation of substrate and surface modes within the sound cone of LiNbO₃. Owing to the periodicity of the PC, periodic boundary conditions are applied along the x_1 and the x_2 directions. A stress free boundary condition is imposed on the top $+x_3$ surface. Note that the presented results were obtained by considering a stress free boundary condition on the bottom surface. No significant difference was found in the frequency range of interest when the bottom surface was clamped instead. Finally, zero charge electrical boundary conditions are imposed on the top and bottom surfaces.

The governing equations of motion for acoustic waves in LiNbO₃, also called electromechanical wave equations, are given by

$$\begin{aligned} \rho(\mathbf{r}) \frac{\partial^2 u_i}{\partial t^2} - c_{ijkl}(\mathbf{r}) \frac{\partial^2 u_k}{\partial x_j \partial x_l} - e_{kij}(\mathbf{r}) \frac{\partial^2 \phi}{\partial x_k \partial x_j} &= 0, \\ e_{ikl}(\mathbf{r}) \frac{\partial u_k}{\partial x_i \partial x_l} - \varepsilon_{ik}(\mathbf{r}) \frac{\partial^2 \phi}{\partial x_i \partial x_k} &= 0, \end{aligned} \quad (1)$$

with i, j, k , and $l = 1, 2$, and 3 , and where u is the elastic displacement and ϕ is the electric potential. In Eq. (1), c , e , ε , and ρ are the stiffness tensor, the piezoelectric tensor, the permittivity tensor, and the mass density, respectively. They all depend on position \mathbf{r} . Solutions must also satisfy stress free boundary conditions at the interface between LiNbO₃ and air holes. Equation (1) is solved numerically with 3D FEM in conjunction with the boundary conditions described earlier.

To calculate the SAW band structure, we first determined the irreducible Brillouin zone of the PC. As LiNbO₃ is an anisotropic and piezoelectric crystal, the irreducible Brillouin zone depends not only on the symmetry of the PC lattice, as in the case of isotropic materials, but also on the LiNbO₃ crystal symmetry. The irreducible Brillouin zone can thus be determined from the slowness curve for the slowest bulk wave, a plot of the inverse of the acoustic velocity as a function of the direction of propagation. By incorporating the symmetry of the slowness curve for LiNbO₃, shown on the left of Fig. 1(c), to the Brillouin zone of the PC, a hexagon centered at $\mathbf{K} = 0$ with \mathbf{K} the Bloch-Floquet wavevector, the corresponding irreducible Brillouin zone is determined. The obtained irreducible zone is indicated as the grey area on the right of Fig. 1(c). Once the irreducible Brillouin zone is known, the calculation can be performed with \mathbf{K} taken inside it.

The existence of non-radiative SAW complete bandgaps was investigated for two different hole depths: $h = 0.7a$ and $h = 0.9a$. For each depth, the diameter d of the hole was fixed at $0.5a$, the upper limit for a sufficient distance between two adjacent holes for the purpose of technological fabrication. Figure 2 shows the calculated SAW band structure in both cases. In the band structures, black dots identify localized SAW modes that exist below the sound line (i.e., inside the non-radiative region). The sound line is represented with a red color. The region above the sound line (i.e., the sound cone indicated by the patterned area) contains substrate and leaky surface modes that extend both in the PC and in the substrate. The shaded green areas represent the complete SAW bandgaps. Because the sound line limits the (ω, \mathbf{K}) area that defines non-radiative bandgaps, some bandgaps exist only in a restricted part of the Brillouin zone, for instance, only around point J_2 as is clearly apparent in Fig. 2(f). The horizontal dashed line in Fig. 2 is defined by the lowest frequency attained by a bulk wave having its wavevector lying exactly on the Brillouin zone boundary. SAW bandgaps below this dashed-line are omnidirectional since they extend in all propagation directions. It can be seen that such an omnidirectional bandgap exists for both considered values of the depth of the holes.

To investigate further the effect of the geometry of the array of holes on the SAW bandgap, the above calculation was repeated with variable depth h and diameter d of the hole. SAW gap maps were generated, as shown in Fig. 3. Figure 3(a) shows the gap map for the case that the diameter d is kept constant at $d = 0.5a$ while the depth h is continuously increased from $0.5a$ to $1a$. Fig. 3(b) further shows the gap map for the case that the depth h is fixed at $h = 0.9a$ while the diameter d is increased from $0.35a$ to $0.5a$. The case $h > 1a$ was not considered because in general the hole

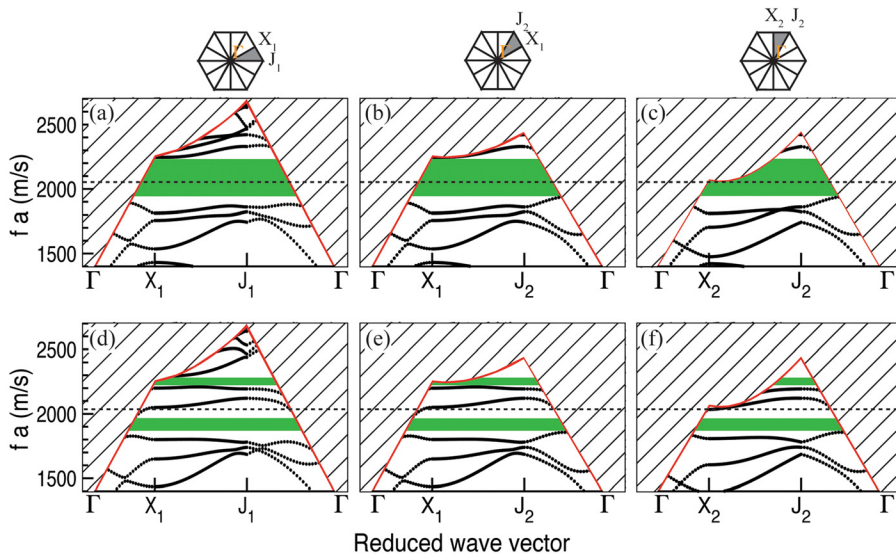


FIG. 2. (Color online) Calculated SAW band structures for the case: $h=0.7a$, $d=0.5a$ (a)-(c), and $h=0.9a$, $d=0.5a$ (d)-(f), obtained for each area inside the irreducible Brillouin zone as indicated by the insets. The black dots, the red lines, and the patterned areas correspond to the localized SAW modes, the sound line, and the substrate or leaky modes, respectively. The shaded green areas indicate SAW bandgaps. The dashed line represents the frequency of the slowest substrate mode with wave vector lying at the Brillouin zone boundary.

depth in the technological fabrication does not go much beyond this range.^{14,15} Our results, however, clearly demonstrate the existence of complete SAW bandgaps for $h < 1a$.

Figure 3(a) shows that from $h=0.5a$ to about $h=0.7a$, the lower frequency gap is widening, and that from $h=0.7a$ to $h=1a$, it is then narrowing and shifting down. At the same time, the higher frequency gap appears only from $h=0.85a$ to $h=1a$. It can be seen that, with respect to the dashed line introduced in the discussion of Fig. 2, only the lower frequency gap is omnidirectional from $h=0.55a$ to $h=1a$. When d is varied with h being fixed at $0.9a$, as shown in Fig. 3(b), we find three different bandgaps. The widest gap is the lowest one when considered at $d=0.5a$. We also

see that when the diameter d is increased, all three gaps are shifting down in frequency and widening at the same time, except the middle gap that vanishes when $d=0.48a$. The only omnidirectional bandgap is the lowest one when considered from $d=0.44a$ to $d=0.5a$.

Until now, the hole constituting the PC structure has been considered to have a cylindrical shape. In reality, however, due to fabrication imperfections, the hole is more likely to have a conical shape^{14,15} with a given slope angle α , as depicted in the inset of Fig. 3(c). The conical shape must affect the bandgap. In order to investigate its effect, we considered α as a variable ranging from 85° to 90° . When $\alpha=90^\circ$, the cylindrical hole considered previously is obtained again. For each value of α , the depth h and the diameter d of the hole were fixed at $0.9a$ and $0.5a$, respectively. The calculated gap map is shown in Fig. 3(c). It can be seen that as the shape of the hole changes from conical to cylindrical, the lower bandgap shifts down in frequency and that the higher gap emerges only above 88° . The lower bandgap is always omnidirectional, and it is completely below the dashed line introduced in the discussion of Fig. 2. The higher bandgap always lies above the dashed-line and is, therefore, only directional.

As a conclusion, we have identified non-radiative complete SAW bandgaps for monolithic piezoelectric phononic crystals composed of finite-depth air holes arrays arranged according to a honeycomb lattice on a semi-infinite LiNbO₃ substrate. Bandgaps were determined from the SAW band structure calculated using 3D FEM, with the anisotropy and piezoelectricity of LiNbO₃ included in the definition of the relevant irreducible Brillouin zone. The non-radiative band-gaps that are obtained are located under the sound cone of the LiNbO₃ substrate. In addition to omnidirectional bandgaps, directional bandgaps are found as well for given parameters and shapes of the hole.

This work is funded by ANR (P3N2009) within Project No. ANR-09-NANO-004 (phoXcry).

¹M. S. Kushwaha, P. Halevi, L. Dobrzynski, and B. Djafari-Rouhani, *Phys. Rev. Lett.* **71**, 2022 (1993).

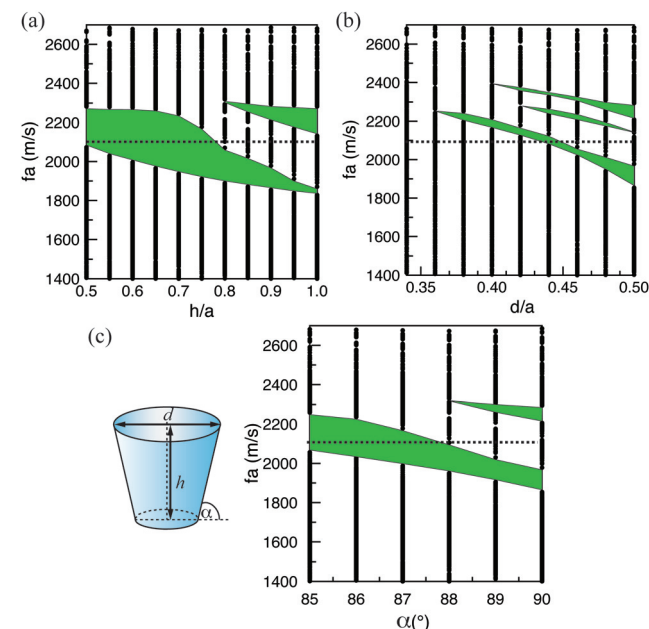


FIG. 3. (Color online) Calculated SAW gap maps for the case when the depth h is varied from $5a$ to $1a$ while the diameter d is fixed at $d=0.5a$ (a), and when the diameter d is varied from $0.34a$ to $0.5a$ while the depth h is fixed at $h=0.9a$ (b). (c) Calculated SAW gap map for the case when the shape of the hole is changing from conical to cylindrical by varying angle α from 85° to 90° , with $h=0.9a$ and $d=0.5a$. The inset illustrates the shape of the conical hole.

- ²M. Sigalas and E. N. Economou, *Solid State Commun.* **86**, 141 (1993).
- ³J. Hwan Oh, I. Kyu Lee, P. Sik Ma, and Y. Young Kim, *Appl. Phys. Lett.* **99**, 083505 (2011).
- ⁴N. Fang, D. Xi, J. Xu, M. Ambati, W. Srituravanich, C. Sun, and X. Zhang, *Nature Mater.* **5**, 452 (2006).
- ⁵R. Wilson, J. Reboud, Y. Bourquin, S. L. Neale, Y. Zhang, and J. M. Cooper, *Lab Chip* **11**, 323 (2010).
- ⁶M. Maldovan and E. L. Thomas, *Appl. Phys. Lett.* **88**, 251907 (2006).
- ⁷S. Sadat-Saleh, S. Benchabane, F. I. Baida, M.-P. Bernal, and V. Laude, *J. Appl. Phys.* **106**, 074912 (2009).
- ⁸Y. Pennec, B. D. Rouhani, E. H. El Boudouti, C. Li, Y. El Hassouani, J. O. Vasseur, N. Papanikolaou, S. Benchabane, V. Laude, and A. Martinez, *Opt. Express* **18**, 14301 (2010).
- ⁹S. Mohammadi, A. A. Eftekhar, A. Khelif, H. Moubchir, R. Westafer, W. D. Hunt, and A. Adibi, *Electron. Lett.* **43**, 898 (2007).
- ¹⁰Y. Pennec, B. Djafari Rouhani, H. Larabi, A. Akjouj, J. N. Gillet, J. O. Vasseur, and G. Thabet, *Phys. Rev. B* **80**, 144302 (2009).
- ¹¹D. Yudistira, S. Benchabane, D. Janner, and V. Pruneri, *Appl. Phys. Lett.* **95**, 052901 (2009).
- ¹²Y. Tanaka and S. Tamura, *Phys. Rev. B* **58**, 7958 (1998).
- ¹³V. Laude, M. Wilm, S. Benchabane, and A. Khelif, *Phys. Rev. E* **71**, 036607 (2005).
- ¹⁴S. Benchabane, A. Khelif, J.-Y. Rauch, L. Robert, and V. Laude, *Phys. Rev. E* **73**, 065601 (2006).
- ¹⁵S. Benchabane, G. Ulliac, O. Gaiffe, R. Salut, Y. Achaoui, and V. Laude, *Appl. Phys. Lett.* **98**, 171908 (2011).
- ¹⁶A. Khelif, Y. Achaoui, S. Benchabane, V. Laude, and A. Boujema, *Phys. Rev. B* **81**, 214303 (2010).
- ¹⁷M. B. Assouar and M. Oudich, *Appl. Phys. Lett.* **99**, 123505 (2011).